International Journal of Thermal Sciences 48 (2009) 2063–2073

Contents lists available at ScienceDirect

International Journal of Thermal Sciences

journal homepage: www.elsevier.com/locate/ijts

Natural convection of water-based nanofluids in an inclined enclosure with a heat source

Elif Büyük Öğüt*

Vocational School of Gebze, Kocaeli University, 41420 Gebze-Kocaeli, Turkey

ARTICLE INFO

Article history:
Received 13 November 2008
Received in revised form
13 March 2009
Accepted 25 March 2009
Available online 17 April 2009

Keywords:
Natural convection
Nanofluid
Inclined enclosure
PDQ
Constant heat flux

ABSTRACT

This study investigates natural convection heat transfer of water-based nanofluids in an inclined square enclosure where the left vertical side is heated with a constant heat flux, the right side is cooled, and the other sides are kept adiabatic. The governing equations are solved using polynomial differential quadrature (PDQ) method. Calculations were performed for inclination angles from 0° to 90°, solid volume fractions ranging from 0% to 20%, constant heat flux heaters of lengths 0.25, 0.50 and 1.0, and a Rayleigh number varying from 10^4 to 10^6. The ratio of the nanolayer thickness to the original particle radius is kept at a constant value of 0.1. The heat source is placed at the center of the left wall. Five types of nanoparticles are taken into consideration: Cu, Ag, CuO, Al_2O_3, and TiO_2. The results show that the average heat transfer rate increases significantly as particle volume fraction and Rayleigh number increase. The results also show that the length of the heater is also an important parameter affecting the flow and temperature fields. The average heat transfer decreases with an increase in the length of the heater. As the heater length is increased, the average heat transfer rate starts to decrease for a smaller inclination angle (it starts to decrease with inclination at 90° for $\varepsilon = 0.25$, 60° for $\varepsilon = 0.50$, 45° for $\varepsilon = 1.0$, respectively).

1. Introduction

In order to manage the growing demand from a variety of industries (electronics, automotive and aerospace industries, for example), heat exchanger devices have to become smaller in size and lighter in weight, and they must provide ever higher performance. Fluids in common use, such as water oil and ethylene glycol, often have low thermal conductivity of conventional heat transfer, a primary limitation in enhancing the performance and the compactness of many electronic devices for engineering applications. To overcome this impediment, there is a strong motivation to develop fluids with advanced heat transfer properties and, in particular, substantially higher conductivities. One innovative way to improve the thermal conductivity of a fluid is to suspend metallic nanoparticles within it. The resulting mixture, referred to as a nanofluid, possesses a substantially larger thermal conductivity than that typical of traditional fluids [1]. Choi [2] was the first to use the term "nanofluid" to refer to a fluid in which nanoparticles are suspended. The term "nanofluid" does not simply refer to a specific liquid–solid mixture, but also to the necessity of other special characteristics, such as even suspension, stable suspension, durable suspension, low agglomeration of particles, and no chemical change of the fluid. Keblinski et al. [3] proposed that the thermal conductivity increase of nanofluids is due to the Brownian motion of particles, the molecular-level layering of the liquid at the liquid/particle interface, the nature of heat transport in the nanoparticles, and the effect of nanoparticle clustering.

One of the most significant parameters regarding the enhancement of heat transfer of nanofluids is the effective thermal conductivity of the nanofluid. Since there is currently a lack of sophisticated theories for predicting the effective thermal conductivity of a nanofluid, several researchers have proposed different correlations to predict the apparent thermal conductivity of two-phase mixtures. The models proposed by Hamilton and Crosser [4], Wasp [5], Maxwell-Garnett [6], Bruggeman [7] and Wang et al. [8] are all meant to determine the effective thermal conductivity of a nanofluid, but all have failed to predict it accurately. To be specific, experimental results have shown much higher thermal conductivities than those predicted by these models. An alternative expression for calculating the effective thermal conductivity of solid–liquid mixtures was proposed by Yu and Choi [9]. They claimed that a structural model of nanofluids might consist of a bulk liquid, solid nanoparticles and solid-like

* Tel./fax: +90 262 7423290.
E-mail address: elif.ogut@kocaeli.edu.tr

1290-0729/$ – see front matter © 2009 Elsevier Masson SAS. All rights reserved.
doi:10.1016/j.ijthermalsci.2009.03.014

Nomenclature

c_p	specific heat at constant pressure
g	gravitational acceleration
Gr	Grashof number
H	height of the enclosure
k	thermal conductivity
L	width of the enclosure
Nu	Nusselt number
p	pressure
Pr	Prandtl number
q	heat flux
R	residue
Ra	Rayleigh number
T	temperature
u	velocity component in the x direction
v	velocity component in the y direction
w	length of heat source
x	cartesian coordinate
y	cartesian coordinate

Greek symbols

α	thermal diffusivity
η	ratio of the nanolayer thickness to the original particle radius
β	thermal expansion coefficient
γ	kinematic viscosity
ε	dimensionless length of the heat source
ξ	outward variable normal to the surface
ϕ	solid volume fraction
μ	dynamic viscosity
φ	inclination angle
ρ	density
ψ	stream function
ω	vorticity

Subscripts

a	average
c	cold
eff	effective
f	fluid
o	reference value
s	solid

Superscript

*	dimensional variable

nanolayers. The solid-like nanolayer acts as a thermal bridge between the solid nanoparticles and the bulk liquid. This is the model that has been used in this study to determine the effective thermal conductivity of a nanofluid.

The past decade has witnessed several studies of convective heat transfer in nanofluids. Khanafer et al. [10] were the first to investigate the problem of buoyancy-driven heat transfer enhancement of nanofluids in a two-dimensional enclosure. Jou and Tzeng [11] numerically investigated the heat transfer performance of nanofluids inside two-dimensional rectangular enclosures. Their results show that increasing the volume fraction causes a significant increase in the average heat transfer coefficient. Santra et al. [12] have conducted a similar kind of study, up to $\phi = 10\%$, using the models proposed by Maxwell-Garnett [6] and Bruggeman [7]. Their results show that the Bruggemann model [7] predicts higher heat transfer rates than the Maxwell-Garnett model [6]. Hwang et al. [13] have carried out a theoretical investigation of the thermal characteristics of natural convection of an alumina-based nanofluid in a rectangular cavity heated from below using Jang and Choi's model [14] for predicting the effective thermal conductivity of nanofluids (and various models for predicting the effective viscosity). Oztop and Abu-Nada [15] investigated heat transfer and fluid flow due to buoyancy forces in a partially heated enclosure using nanofluids using various types of nanoparticles. It was found that the heat transfer enhancement due to using a nanofluid is more pronounced at a low aspect ratio than at a high aspect ratio.

Natural convection heat transfer in a partially heated enclosure is an issue of practical importance. Air-cooling is one of the preferred methods for cooling computer systems and other electronic equipments, due to its simplicity and low cost. The electronic components are treated as heat sources embedded on flat surfaces [16]. In many applications, natural convection is the only feasible mode of cooling such sources.

For conventional fluids, convective heat transfer in a partially heated enclosure has been studied in the literature. A numerical study on natural convection in a glass-melting tank heated locally from below has been performed by Sarris et al. [17]. More recently, Calcagni et al. [18] made an experimental and numerical study of free convective heat transfer in a square enclosure characterized by a discrete heater located on the lower wall and cooling from the lateral walls. A numerical investigation of the natural convection of air in a vertical square cavity with localized isothermal heating from below and symmetrical cooling from the sidewalls was carried out by Aydin and Yang [19]. The top wall as well as the non-heated parts of the bottom wall were considered to be adiabatic. Sharif and Mohammad [20] studied the same configuration as Aydin and Yang, [19] where the localized isothermal heat source at the bottom wall is replaced with a constant flux heat source, a scenario that is physically more realistic for electronic component cooling applications. They investigated the effect of aspect ratio and inclination of the cavity on the heat transfer process. Cheikh et al. [21] studied the natural convection cooling of a localized heated plate embedded symmetrically at the bottom of an air-filled square enclosure.

The problem of natural convection heat transfer of nanofluids in an enclosure with a constant flux heater has not yet been analyzed.

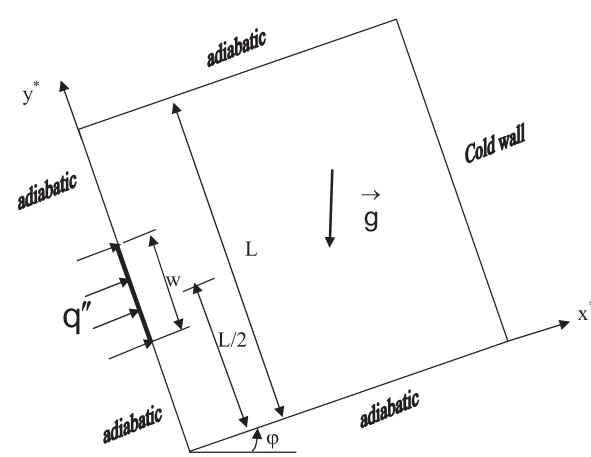

Fig. 1. Geometry and coordinate system.

Table 1
Thermophysical properties of base fluid and nanoparticles.

Property	Water	Cu	Ag	CuO	Al_2O_3	TiO_2
ρ (kg/m^3)	997.1	8933	10,500	6500	3970	4250
c_p (J/kg K)	4179	385	235	535.6	765	686.2
k (W/m K)	0.613	400	429	20	40	8.9538
$\alpha \times 10^7$ (m^2/s)	1.47	1163.1	1738.6	57.45	131.7	30.7
β (K^{-1})	0.00021	0.000051	0.000054	0.000051	0.000024	0.000024

Table 2
Grid independency for water-based copper nanofluid at $\varphi = 0°$ and $Ra = 10^6$.

ε	ϕ		31 × 31	36 × 36	41 × 41	46 × 46	51 × 51
0.25	0.0	Nu_a	11.6984	11.6765	11.6618	11.6499	11.6412
		$\lvert\psi\rvert_{max}$	−7.9872	−7.5917	−7.5971	−7.9870	−7.5974
	0.20	Nu_a	18.0857	18.0574	18.0372	18.0221	18.0103
		$\lvert\psi\rvert_{max}$	−15.0347	−14.5124	−14.3418	−14.1201	−13.8274

Table 3
Validation of the numerical code.

	$Ra = 10^4$		$Ra = 10^5$		$Ra = 10^6$	
	de Vahl Davis [34]	Present	de Vahl Davis [34]	Present	de Vahl Davis [34]	Present
Nu_a	2.24	2.24	4.52	4.52	8.80	8.82
Nu_{max}	3.53	3.53	7.72	7.70	17.93	17.56
Nu_{min}	0.59	0.59	0.73	0.73	0.99	0.98

The present study therefore aims to investigate this problem and find the effects of varying the solid volume fraction (φ), nanoparticle type, inclination angle, heater length and Rayleigh number (Ra) on flow and heat transfer.

2. Analysis

The geometry of the present problem is shown in Fig. 1. An inclined square enclosure of width L is investigated, where the left vertical wall is heated with constant heat flux both partially and throughout the entire wall, with the right wall cooled to T_c and other sides kept adiabatic. The flow is assumed to be Newtonian, two-dimensional, steady and incompressible. It is also assumed that the base fluid and the nanoparticles are in thermodynamic equilibrium and that they flow at the same velocity.

The thermophysical properties of the nanofluid are assumed to be constant except for the density variation in the buoyancy force, which is estimated based on the Boussinesq approximation. Under the assumption of constant thermal properties, the Navier–Stokes equations for steady two-dimensional flow are

Continuity equation:

$$\frac{\partial u^*}{\partial x^*} + \frac{\partial v^*}{\partial y^*} = 0 \tag{1}$$

x-momentum equation:

$$\left(u^*\frac{\partial u^*}{\partial x^*} + v^*\frac{\partial u^*}{\partial y^*}\right) = -\frac{1}{\rho_{nf,0}}\frac{\partial p^*}{\partial x^*} + \frac{\mu_{eff}}{\rho_{nf,0}}\left(\frac{\partial^2 u^*}{\partial x^{*2}} + \frac{\partial^2 u^*}{\partial y^{*2}}\right) + \frac{1}{\rho_{nf,0}}(\rho\beta)_{nf} g \sin\varphi (T - T_C) \tag{2}$$

y-momentum equation:

$$\left(u^*\frac{\partial v^*}{\partial x^*} + v^*\frac{\partial v^*}{\partial y^*}\right) = -\frac{1}{\rho_{nf,0}}\frac{\partial p^*}{\partial y^*} + \frac{\mu_{eff}}{\rho_{nf,0}}\left(\frac{\partial^2 v^*}{\partial x^{*2}} + \frac{\partial^2 v^*}{\partial y^{*2}}\right) + \frac{1}{\rho_{nf,0}}(\rho\beta)_{nf} g \cos\varphi (T - T_C) \tag{3}$$

Table 4
Comparison of the average Nusselt number for natural convection of nanofluids in an enclosure.

	Gr/ϕ	0	0.04	0.08	0.12	0.16	0.20
Present	10^3	1.93	2.07	2.21	2.34	2.48	2.63
Khanafer et al. [10]	10^3	1.96	2.11	2.25	2.36	2.57	2.75
Present	10^4	4.07	4.40	4.72	4.87	5.32	5.62
Khanafer et al. [10]	10^4	4.07	4.36	4.68	5.00	5.32	5.68

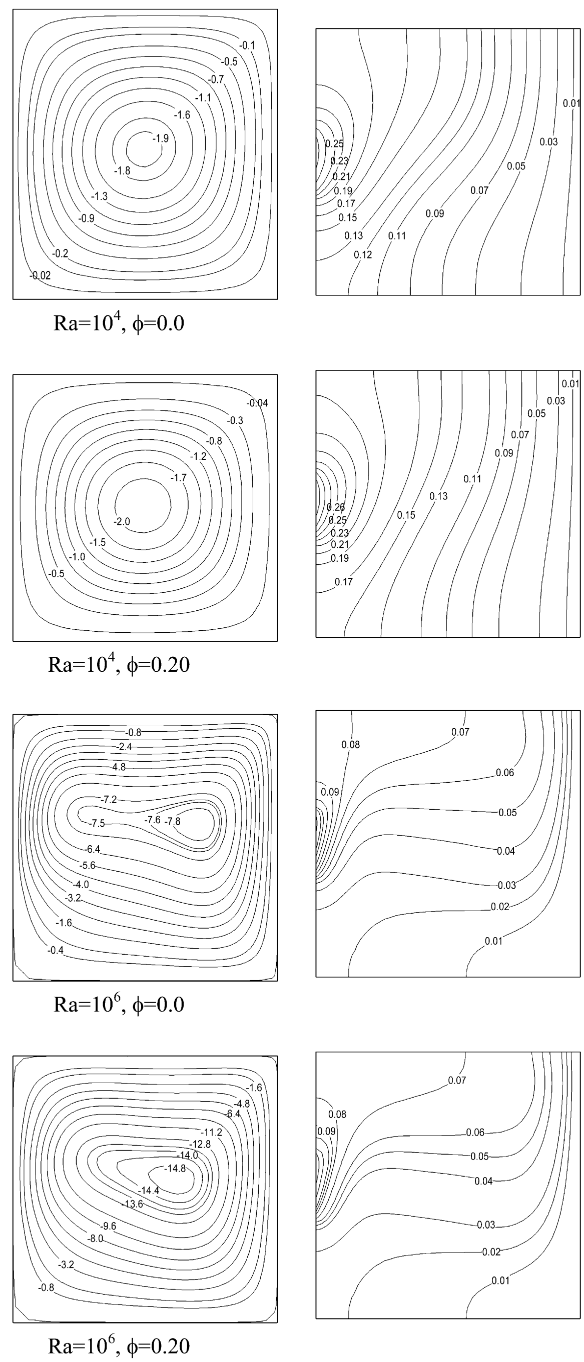

Fig. 2. Streamlines (on the left) and isotherms (on the right) of a copper-based nanofluid for $\varepsilon = 0.25$ and $\varphi = 0°$.

Energy equation:

$$\left(u^*\frac{\partial T}{\partial x^*}+v^*\frac{\partial T}{\partial y^*}\right) = \alpha_{\text{nf}}\left(\frac{\partial^2 T}{\partial x^{*2}}+\frac{\partial^2 T}{\partial y^{*2}}\right) \tag{4}$$

where

$$\alpha_{\text{nf}} = \frac{k_{\text{eff}}}{(\rho c_p)_{\text{nf},0}}$$

The viscosity of the nanofluid can be estimated using the existing relations for the two-phase mixture. The viscosity of the nanofluid containing a dilute suspension of small rigid spherical particles has been given by Brinkman [22]. This relation is used for effective viscosity in this work, as given by

$$\mu_{\text{eff}} = \frac{\mu_{\text{f}}}{(1-\phi)^{2.5}} \tag{5}$$

The effective density of the nanofluid at reference temperature is defined as

$$\rho_{\text{nf,o}} = (1-\phi)\rho_{\text{f,o}}+\phi\rho_{\text{s,o}} \tag{6}$$

and the heat capacitance of the nanofluid and part of Boussinesq term are defined as

$$(\rho c_p)_{\text{nf}} = (1-\phi)\rho_{\text{f}}c_{\text{pf}}+\phi\rho_{\text{s}}c_{\text{ps}} \tag{7}$$

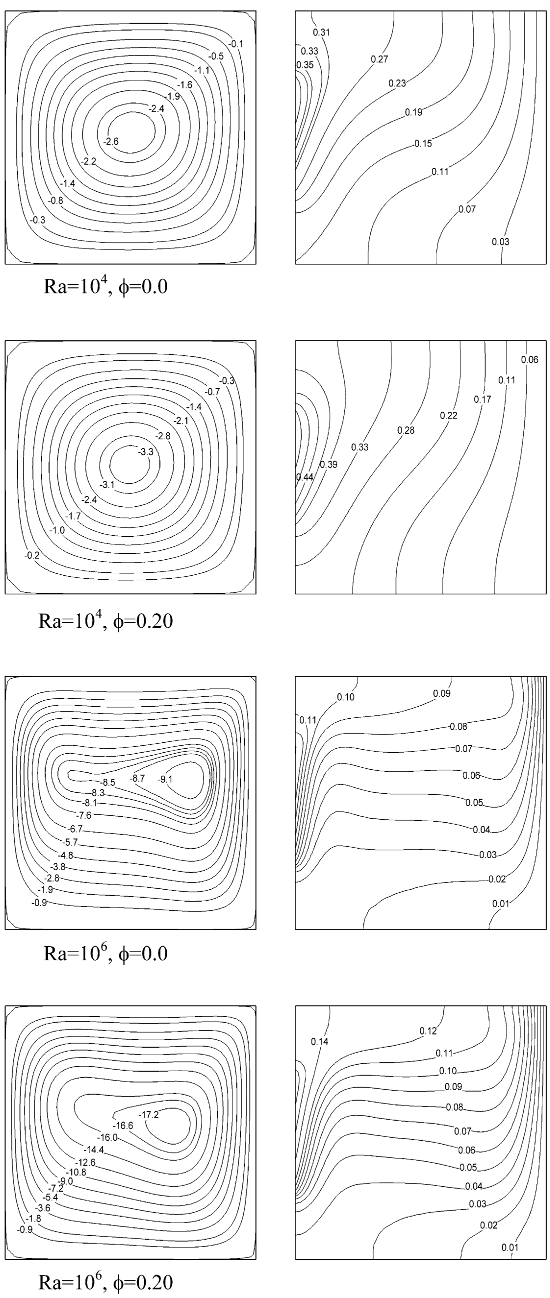

Fig. 3. Streamlines (on the left) and isotherms (on the right) of a copper-based nanofluid for $\varepsilon = 0.50$ and $\varphi = 0°$.

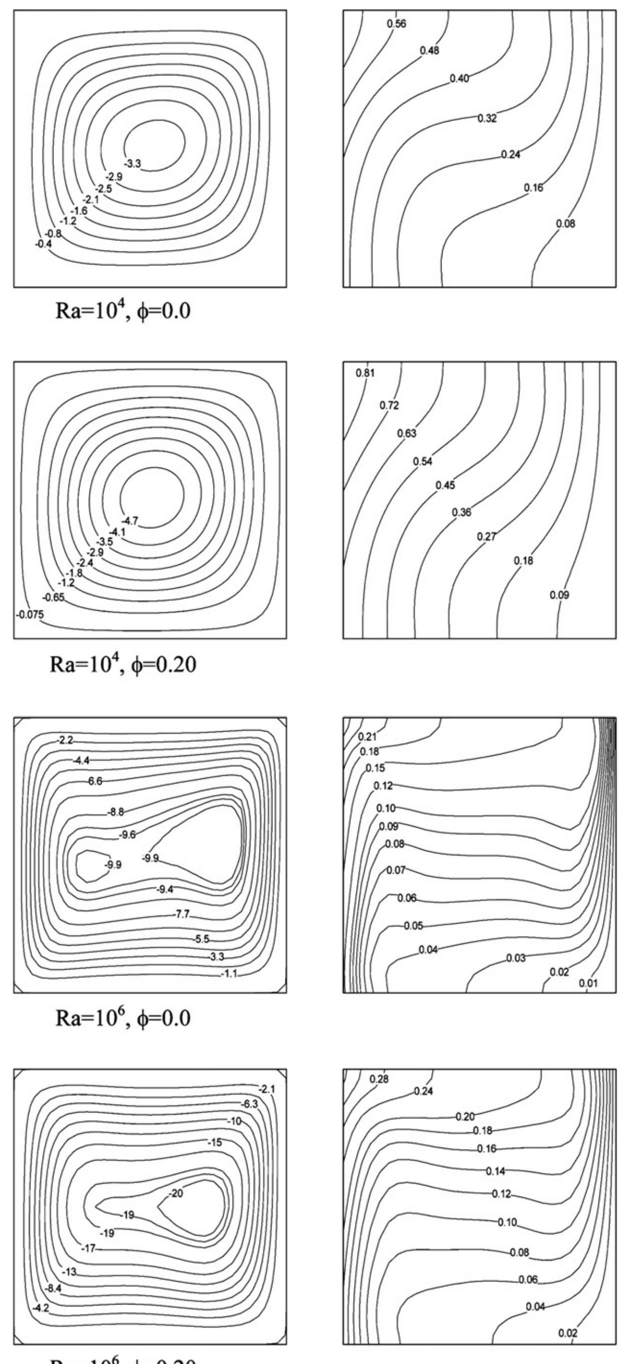

Fig. 4. Streamlines (on the left) and isotherms (on the right) of a copper-based nanofluid for $\varepsilon = 1.0$ and $\varphi = 0°$.

$$(\rho\beta)_{\rm nf} = (1-\phi)\rho_{\rm f}\beta_{\rm f} + \phi\rho_{\rm s}\beta_{\rm s} \tag{8}$$

as given by Xuan and Roetzel [23]. Here, ϕ is the volume fraction of solid particles, and the subscripts f, nf and s stand for base fluid, nanofluid and solid, respectively.

As mentioned above, the correlation proposed by Yu and Choi [9] was used for determining nanofluid effective thermal conductivity. They modified the Maxwell equation for the effective thermal conductivity of a solid–liquid mixture to include the effect of a liquid nanolayer on the surface of a nanoparticle:

$$\frac{k_{\rm eff}}{k_{\rm f}} = \frac{k_{\rm s} + 2k_{\rm f} + 2(k_{\rm s} - k_{\rm f})(1+\eta)^3\phi}{k_{\rm s} + 2k_{\rm f} - (k_{\rm s} - k_{\rm f})(1+\eta)^3\phi} \tag{9}$$

where η is the ratio of the nanolayer thickness to the radius of the original particle.

For comparison purposes, the effective thermal conductivity of a fluid can be determined by Maxwell–Garnett's [6] self-consistent approximation model (the "MG model"). For the two-component spherical-particle suspension, the MG model gives:

$$\frac{k_{\rm eff}}{k_{\rm f}} = \frac{k_{\rm s} + 2k_{\rm f} - 2\phi(k_{\rm f} - k_{\rm s})}{k_{\rm s} + 2k_{\rm f} + \phi(k_{\rm f} - k_{\rm s})} \tag{10}$$

To obtain non-dimensional governing equations, the following dimensionless variables are used:

$$x = \frac{x^*}{L},\ y = \frac{y^*}{L},\ u = \frac{u^*}{\alpha_{\rm f}/L},\ v = \frac{v^*}{\alpha_{\rm f}/L},\ p = \frac{L^2}{\rho_{\rm fo}\alpha_{\rm f}^2}p^*, \tag{11}$$

$$\theta = \frac{T^* - T_{\rm C}}{\Delta T},\ \Delta T = \frac{q''L}{k_{\rm f}} \tag{12}$$

where u^* and v^* are the dimensional velocity components, g is the gravitational acceleration, p^* is the dimensional pressure, T^* is the dimensional temperature, $\rho_{\rm f}$ is the fluid density, $k_{\rm f}$ is the thermal conductivity and $\alpha_{\rm f}$ is the thermal diffusivity of the fluid.

The effects of buoyancy are incorporated in this formulation by invoking the Boussinesq approximation. The viscous dissipation terms and thermal radiation are assumed to be negligible. Using the vorticity-stream function formulation, the dimensionless governing equations can be given as follows for steady state and laminar:

Stream function equation:

$$\frac{\partial^2\psi}{\partial x^2} + \frac{\partial^2\psi}{\partial y^2} = -\omega \tag{13}$$

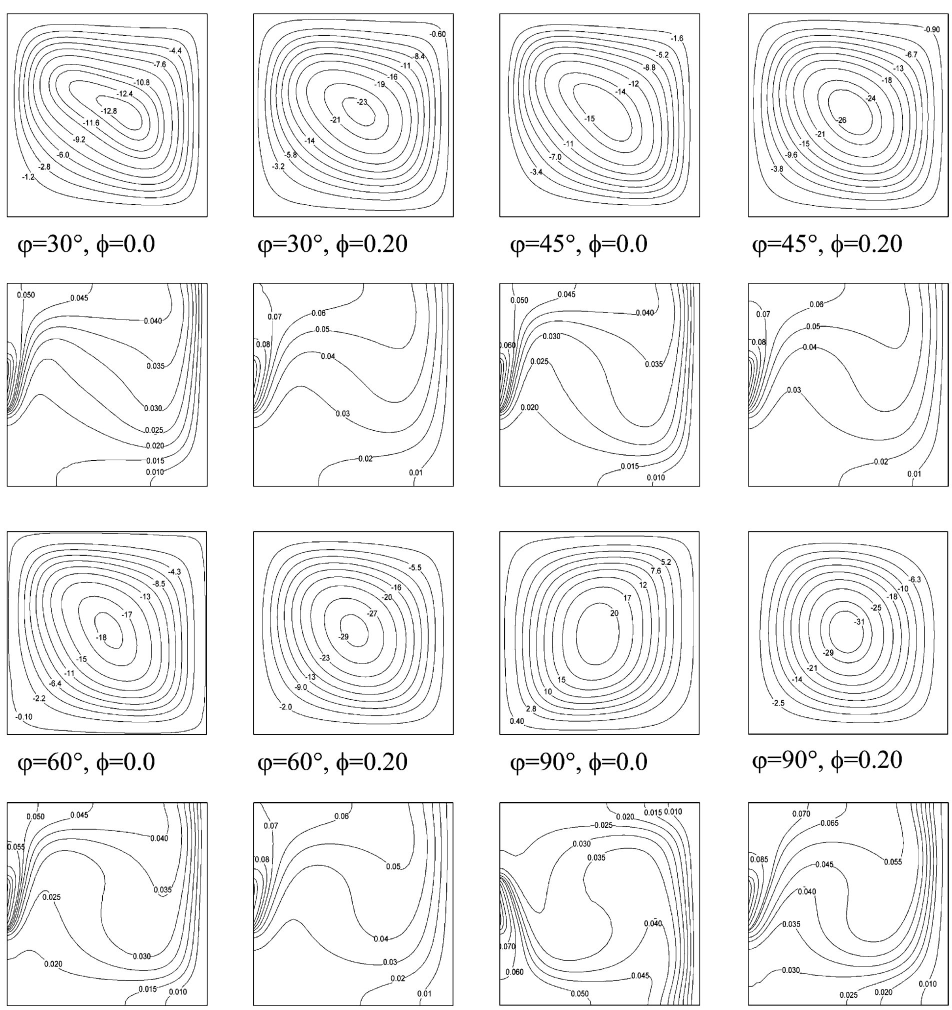

Fig. 5. Streamlines (on the top) and isotherms (on the bottom) of a copper-based nanofluid for various inclination angle at $\varepsilon = 0.25$ and $Ra = 10^6$.

Vorticity transport equation:

$$u\frac{\partial\omega}{\partial x}+v\frac{\partial\omega}{\partial y}=\frac{\nu_{\mathrm{eff}}}{\nu_{\mathrm{f}}}Pr\left(\frac{\partial^2\omega}{\partial x^2}+\frac{\partial^2\omega}{\partial y^2}\right)+\frac{\beta_{\mathrm{nf}}}{\beta_{\mathrm{f}}}Ra\,Pr\left[\cos\varphi\frac{\partial\theta}{\partial x}-\sin\varphi\frac{\partial\theta}{\partial y}\right] \tag{14}$$

Energy equation:

$$u\frac{\partial\theta}{\partial x}+v\frac{\partial\theta}{\partial y}=\frac{\alpha_{\mathrm{nf}}}{\alpha_{\mathrm{f}}}\left[\frac{\partial^2\theta}{\partial x^2}+\frac{\partial^2\theta}{\partial y^2}\right] \tag{15}$$

Here, the Prandtl and Rayleigh numbers are defined as

$$Pr=\frac{\gamma_{\mathrm{f}}}{\alpha_{\mathrm{f}}},\quad Ra=\frac{g\beta_{\mathrm{f}}L^3\Delta T}{\gamma_{\mathrm{f}}\alpha_{\mathrm{f}}} \tag{16}$$

where β is the coefficient of thermal expansion and γ is the kinematic viscosity. ΔT is the temperature scaling defined as $q''L/k_{\mathrm{f}}$.

The dimensionless stream function and vorticity used in Eqs. (13) and (14) are defined as follows:

$$u=\frac{\partial\psi}{\partial y},\quad v=-\frac{\partial\psi}{\partial x},\quad \omega=\frac{\partial v}{\partial x}-\frac{\partial u}{\partial y} \tag{17}$$

The appropriate boundary conditions for the governing equations are

$$\text{On the bottom walls: } \psi(x,0)=0,\ \left.\frac{\partial\theta}{\partial y}\right|_{x,0}=0, \tag{18}$$

$$\text{On the top wall: } \psi(x,1)=0,\ \left.\frac{\partial\theta}{\partial y}\right|_{x,1}=0 \tag{19}$$

$$\text{On the left wall: } \psi(0,y)=0,\ \text{for } 0\le y<(1-\varepsilon)/2, \frac{\partial\theta}{\partial x}=0 \tag{20a}$$

$$\text{for } (1-\varepsilon)/2\le y\le(1+\varepsilon)/2,\quad \frac{\partial\theta}{\partial x}=-1 \tag{20b}$$

$$\text{for } (1+\varepsilon)/2<y\le 1,\quad \frac{\partial\theta}{\partial x}=0 \tag{20c}$$

On the right walls:

$$\psi(1,y)=0,\quad \theta(1,y)=0. \tag{21}$$

where $\varepsilon=w/L$.

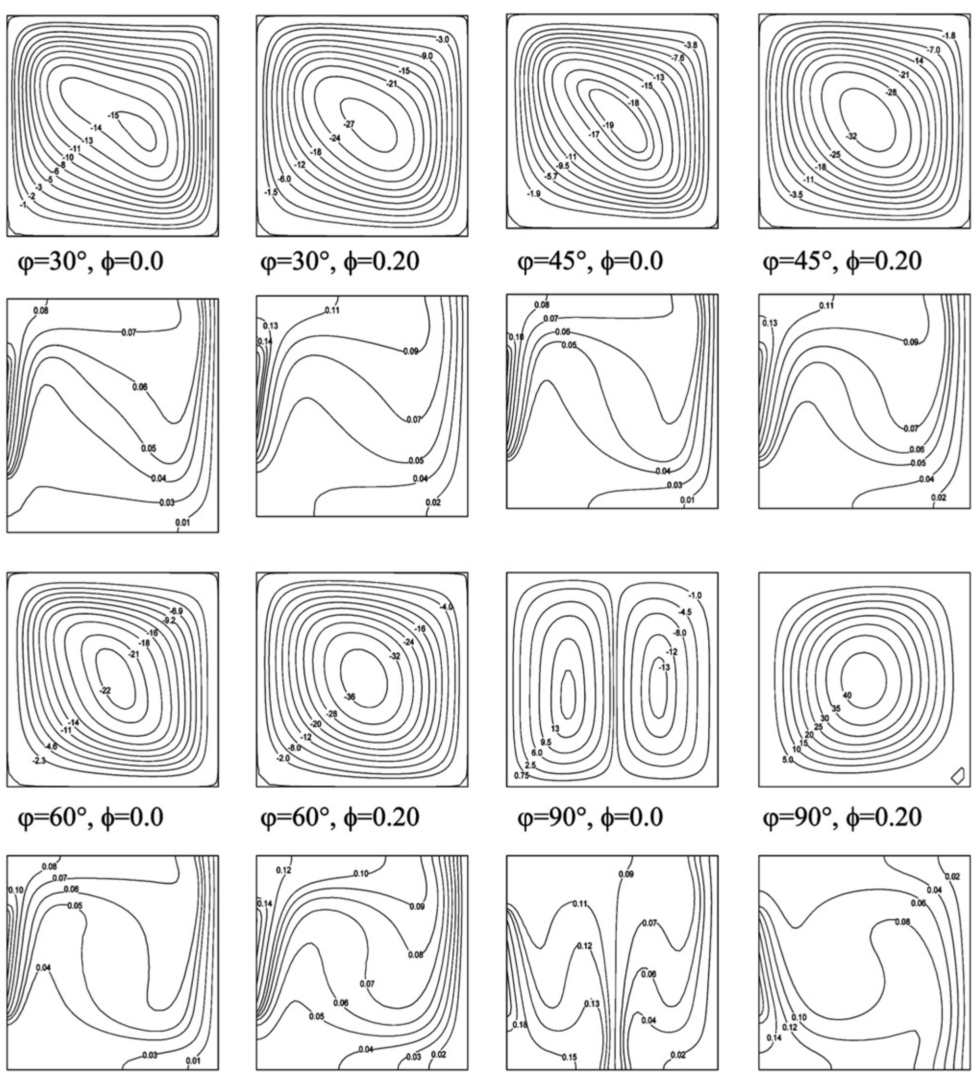

Fig. 6. Streamlines (on the top) and isotherms (on the bottom) of a copper-based nanofluid for various inclination angle at $\varepsilon=0.50$ and $Ra=10^6$.

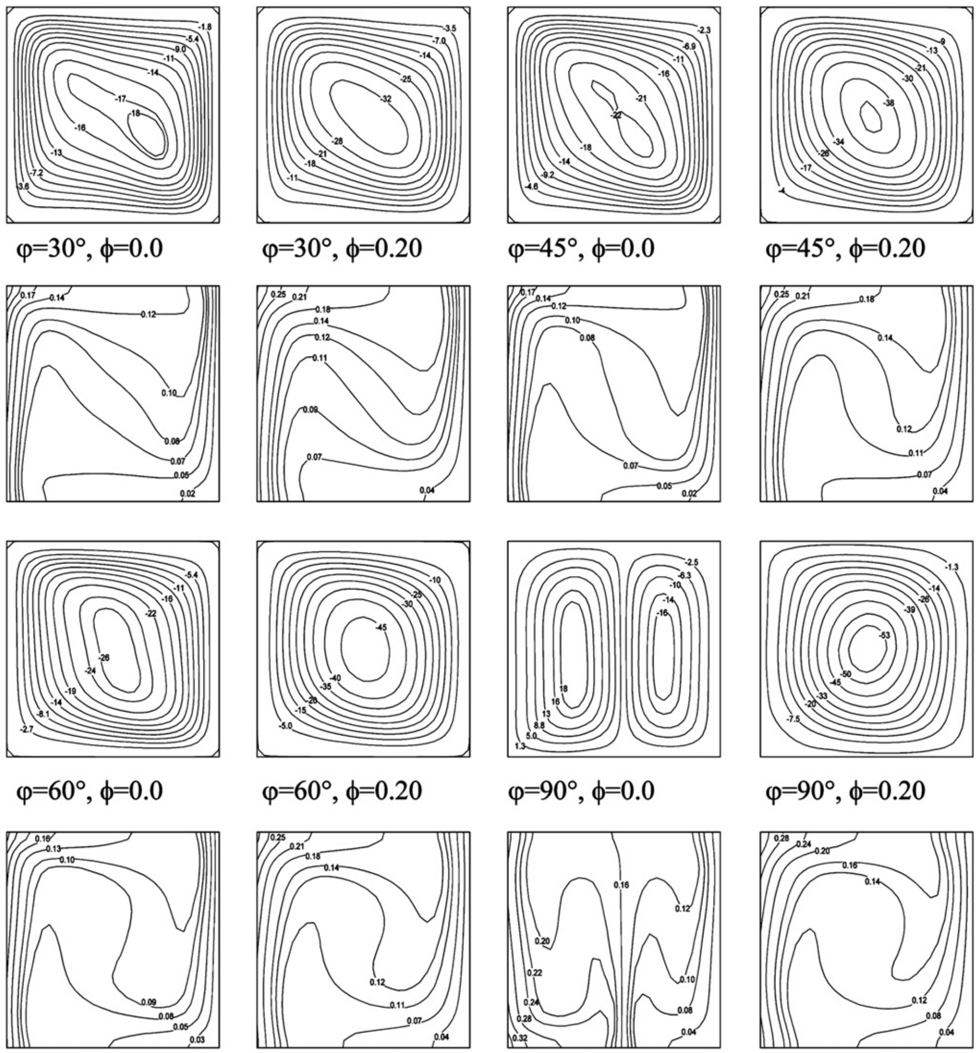

Fig. 7. Streamlines (on the top) and isotherms (on the bottom) of a copper-based nanofluid for various inclination angles at $\varepsilon = 1.0$ and $Ra = 10^6$.

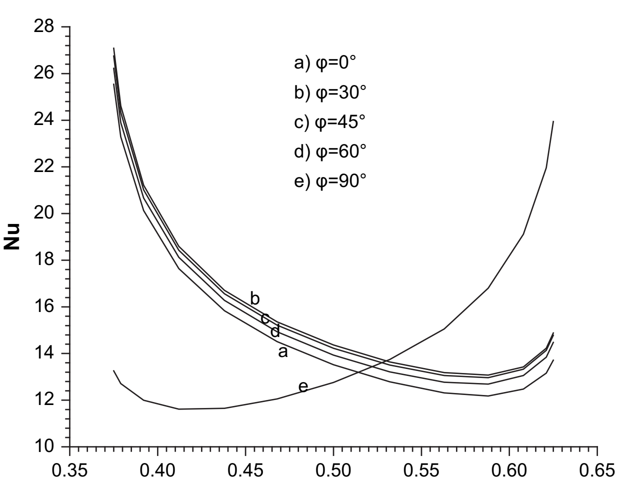

Fig. 8. Variation of the local Nusselt number of a copper-based nanofluid for various inclination angles at $Ra = 10^6$, $\varepsilon = 0.25$ and $\phi = 0.10$.

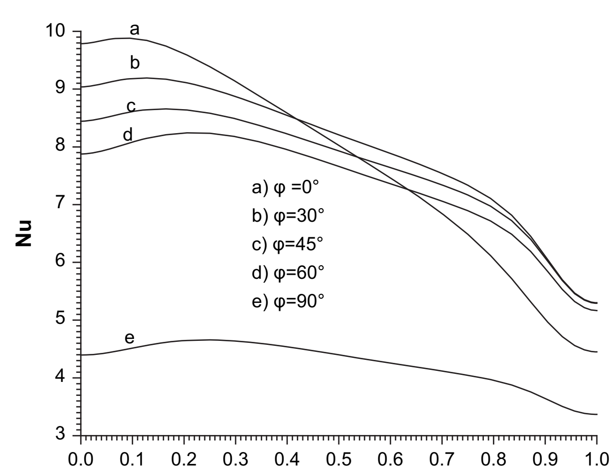

Fig. 9. Variation of the local Nusselt number of a copper-based nanofluid for various inclination angles at $Ra = 10^6$, $\varepsilon = 1.0$ and $\phi = 0.10$.

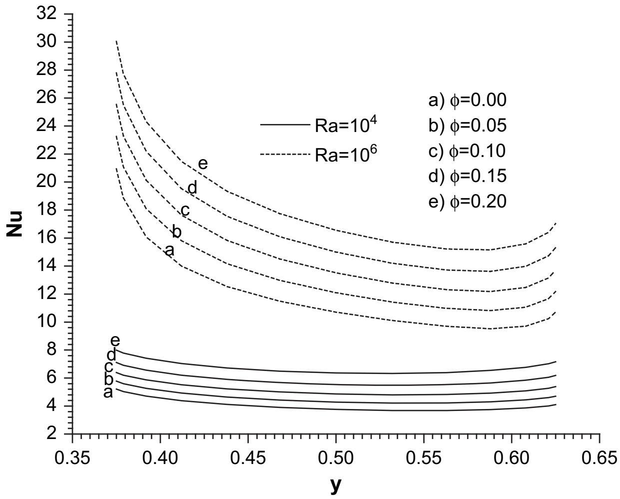

Fig. 10. Variation of the local Nusselt number of a copper-based nanofluid for various volume fractions at $\varepsilon = 0.25$.

Note that there is no physical boundary condition for the value of the vorticity on a solid boundary; however, an expression can be derived from the stream function equation as $\omega_{\text{wall}} = -\partial^2\psi/\partial\xi^2$, where ξ is the direction of the outward normal to the surface.

2.1. Evaluation of heat transfer

The local heat transfer coefficient is defined as

$$h_{\text{y}} = \frac{q''}{(T_{\text{s}}(y) - T_{\text{c}})} \tag{22}$$

where h_{y} represents local heat transfer coefficient and $T_{\text{s}}(y)$ the local temperature at a point on the heated surface. The local and average Nusselt numbers for the wall with constant heat flux are obtained for the nanofluid case using the following relation:

$$Nu = \frac{h_{\text{y}}L}{k_{\text{f}}} = \frac{k_{\text{eff}}}{k_{\text{f}}}\frac{1}{\theta_{\text{s}}(y)}. \tag{23}$$

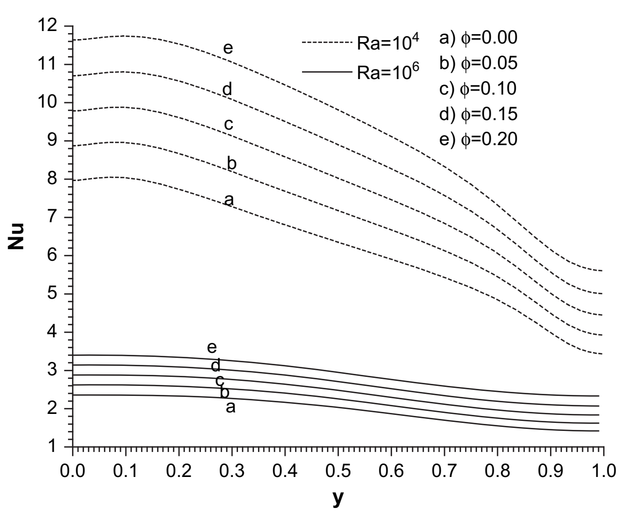

Fig. 11. Variation of the local Nusselt number of a copper-based nanofluid for various volume fractions at $\varepsilon = 1.0$.

The average Nusselt number is defined as

$$Nu_{\text{a}} = \frac{1}{\varepsilon}\int_0^{\varepsilon} Nu\,\mathrm{d}y \tag{24}$$

where $\theta_{\text{s}}(y)$ is the local dimensionless temperature.

3. Numerical method

Polynomial-based differential quadrature (PDQ) is an efficient way to obtain accurate numerical results while using only a very small number of grid points, thus requiring very small computational effort and virtual storage [24–26]. The dimensionless governing equations were therefore solved using the differential

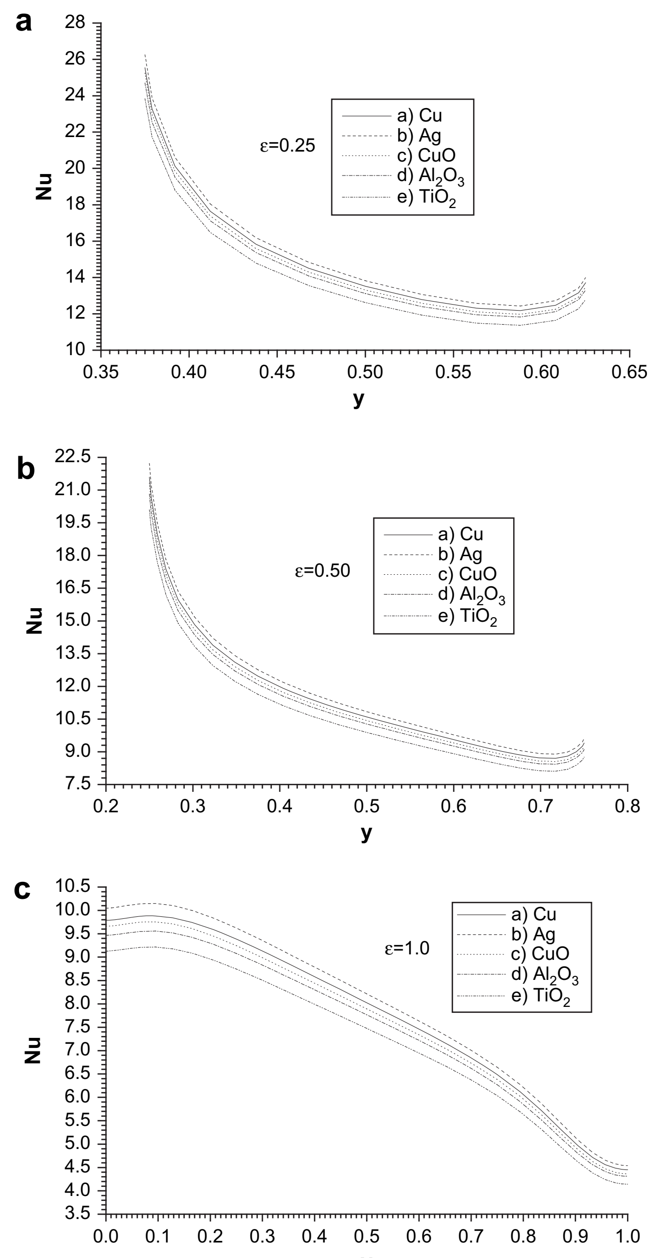

Fig. 12. Variation of the local Nusselt number of different nanoparticles for $Ra = 10^6$ and $\phi = 0.10$, a) $\varepsilon = 0.25$, b) $\varepsilon = 0.50$, and c) $\varepsilon = 1.0$.

quadrature method. The PDQ method was used to transform the governing equations into a set of algebraic equations using the following non-uniform Chebyshev–Gauss–Lobatto grid point distribution [27–33]:

$$x_i = \frac{1}{2}\left[1-\cos\left(\frac{i}{N}\pi\right)\right], \ i = 0,1,2,\ldots,N$$
$$y_j = \frac{1}{2}\left[1-\cos\left(\frac{j}{M}\pi\right)\right], \ j = 0,1,2,\ldots,M \tag{25}$$

The points in this grid system are more closely spaced in regions near the walls where large velocity and temperature gradients are expected to develop. The computational results were obtained by the successive over-relaxation (SOR) iteration method. The convergence criteria were chosen as $|R|_{\max} \le 10^{-5}$, where $|R|_{\max}$ is the maximum absolute residual value for the vorticity, stream function, and temperature equations.

3.1. Grid independence study

Here, solutions for various mesh sizes have been studied in order to determine independence of each solution on the detailed form of the grid. The results show that solutions obtained with more than 31×31 mesh points for $\varepsilon = 1$ and more than 51×51 mesh points for $\varepsilon = 0.25$ and $\varepsilon = 0.50$ are sufficient for grid independence. Results for $\varphi = 0°$, $\varepsilon = 0.25$ and $Ra = 10^6$ are shown in Table 2. Given these findings, these minimal acceptable numbers of mesh points have been chosen for this study. The enclosure was modeled with three separate meshes (covering three different regions in vertical direction) for the case where heat flux is applied partially through the left wall.

3.2. Validation of the code

The results obtained by the code used here are validated by the findings of de Vahl Davis [34] for different values of *Ra* and have been summarized in Table 3. The difference between the average Nusselt number found by de Vahl Davis [34] and that obtained by the present code is well within the acceptable limit. Moreover, the results of the present numerical code can also be validated by the findings of Khanafer et al. [10], who studied natural convection heat transfer of water-based copper nanofluids for an enclosure with isothermally heated sidewalls and adiabatic horizontal walls (see Table 4).

4. Results and discussion

The natural convection heat transfer of water-based nanofluids in an inclined enclosure with a constant heat flux heater has been investigated numerically in this study. The computational results were obtained for inclination angles ranging from 0° to 90°, for Rayleigh numbers varying from 10^4 to 10^6 and for three different lengths of the heat source (0.25, 0.50, and 1.0). The Prandtl number of the base fluid (water) is 6.2, and the nanoparticle volume fraction ϕ was, variably, 0%, 8%, 16%, and 20%. The value of η, the ratio of the nanolayer thickness to the original particle radius, is held fixed at 0.1. Five types of nanoparticles were studied: Cu, Ag, CuO, Al_2O_3, and TiO_2. The corresponding thermophysical properties of the fluid and solid phases are shown in Table 1.

The flow and energy transport in the enclosure for the water-based copper nanofluid case are shown in Figs. 2–4 for various lengths of the heat source, solid volume fractions and the Rayleigh numbers at the inclination angle $\varphi = 0°$. The flow is single-cellular for low Rayleigh numbers ($Ra = 10^4$). Secondary cells occur in the central region with increasing Rayleigh number. At higher *Ra*, the center cell becomes egg-shaped, and the isotherm patterns change significantly, indicating that convection is the dominant mechanism for heat transfer in the cavity. As solid volume fraction increases, heat deformations are pressurized, and the flow becomes single-cellular again because of increasing energy exchange. Figs. 2–4 also show that the intensity of the streamlines increases with an increase in the volume fraction as a result of high-energy transport through the ultrafine particles. When the heat source length ε increases, more heat is transferred into the system and thus the temperature of the entire cavity increases.

The streamlines and isotherms in the enclosure for the water-based copper nanofluid case are shown in Figs. 5–7 for various values of inclination angles, lengths of the heat source and solid volume fractions at $Ra = 10^6$. Thermal stratification in the core region is reduced with increasing inclination angle, resulting in a stronger flow field.

In the case of a heater of length $\varepsilon = 0.25$, secondary cells are seen to disappear when the enclosure is inclined and the remaining cells return to having an elliptical shape oriented along the symmetry axis.

The changes in local Nusselt number for water-based copper nanofluids at the heated wall are shown in Figs. 8 and 9 for different angles of inclination. The local Nusselt number is at a maximum for

Table 5
Average Nusselt number for inclination angle $\varphi = 0°$.

Material		Cu			Ag			CuO			Al_2O_3			TiO_2		
ε	ϕ\Ra	10^4	10^5	10^6	10^4	10^5	10^6	10^4	10^5	10^6	10^4	10^5	10^6	10^4	10^5	10^6
0.25	0.00	3.9907	6.8897	11.6412	3.9907	6.8897	11.6412	3.9907	6.8897	11.6412	3.9907	6.8897	11.6412	3.9907	6.8897	11.6412
	0.05	4.5313	7.7560	13.1543	4.5790	7.8506	13.3012	4.4856	7.6858	13.0383	4.4585	7.6207	12.9491	4.3669	7.4725	12.6920
	0.10	5.1322	8.6458	14.7090	5.2274	8.8567	15.0392	5.0309	8.5061	14.4832	4.9866	8.3570	14.2731	4.7839	8.0471	13.7345
	0.15	5.8312	9.5687	16.3205	5.9653	9.9200	16.8766	5.6545	9.3588	15.9889	5.6174	9.1077	15.6264	5.2712	8.6168	14.7725
	0.20	6.6804	10.5374	18.0103	6.8368	11.0559	18.8420	6.3924	10.2541	17.5731	6.4031	9.8849	17.0257	5.8635	9.1871	15.8117
0.50	0.00	2.9013	5.2452	8.9791	2.9013	5.2452	8.9791	2.9013	5.2452	8.9791	2.9013	5.2452	8.9791	2.9013	5.2452	8.9791
	0.05	3.2410	5.8896	10.1371	3.2850	5.9639	10.2543	3.2131	5.8379	10.0453	3.1803	5.7853	9.9701	3.1200	5.67412	9.7736
	0.10	3.5942	6.5434	11.3238	3.6875	6.7099	11.5868	3.5375	6.4429	11.1455	3.4696	6.3208	10.9708	3.3418	6.0901	10.5594
	0.15	3.9767	7.2106	12.5468	4.1213	7.4896	12.9892	3.8860	7.0637	12.2883	3.7892	6.8545	11.9895	3.5801	6.4927	11.3384
	0.20	4.4151	7.8956	13.8171	4.6058	8.3117	14.4791	4.2764	7.7045	13.4844	4.1699	7.3895	13.0363	3.85532	6.8819	12.1137
1.0	0.00	1.9485	3.53415	6.2093	1.9485	3.53415	6.2093	1.9485	3.53415	6.2093	1.9485	3.53415	6.2093	1.9485	3.53415	6.2093
	0.05	2.1752	3.9365	6.9836	2.2055	3.9873	7.0698	2.1569	3.9023	6.9213	2.1340	3.8658	6.8618	2.0941	3.7921	6.7290
	0.10	2.4039	4.3680	7.7730	2.4703	4.4803	7.9647	2.3680	4.3019	7.6525	2.3169	4.2194	7.5169	2.2341	4.0657	7.2395
	0.15	2.6388	4.8111	8.5813	2.7466	4.9970	8.9014	2.5853	4.7144	8.4086	2.5031	4.5765	8.1805	2.3720	4.3345	7.7427
	0.20	2.8876	5.2708	9.4142	3.0410	5.5447	9.8898	2.8143	5.1439	9.1959	2.7034	4.9404	8.8589	2.5145	4.5991	8.2404

Table 6
Average Nusselt number for different inclination angle at $Ra = 10^6$.

Material		Cu			Ag			CuO			Al_2O_3			TiO_2		
ε	$\varphi \backslash \phi$	0.0	0.10	0.20	0.0	0.10	0.20	0.0	0.10	0.20	0.0	0.10	0.20	0.0	0.10	0.20
0.25	30°	12.2908	15.6324	19.3411	12.2908	15.9450	20.1390	12.2908	15.4049	18.8812	12.2908	15.2391	18.4260	12.2908	14.6513	17.0834
	45°	12.1008	15.4872	19.3088	12.1008	15.7787	20.0667	12.1008	15.2539	18.8158	12.1008	15.1158	18.4184	12.1008	14.5250	17.0588
	60°	11.7900	15.1886	19.0437	11.7900	15.4711	19.7817	11.7900	14.9377	18.5062	11.7900	14.8077	18.1345	11.7900	14.2234	16.7834
	90°	10.6584	13.9613	17.6711	10.6584	14.2323	18.3673	10.6584	13.6613	17.0446	10.6584	13.5170	16.6778	10.6584	12.9758	15.4171
0.50	30°	9.3202	11.8012	14.5202	9.3202	12.0457	15.1341	9.3202	11.6365	14.2045	9.3202	11.5013	13.8545	9.3202	11.0613	12.8499
	45°	9.0675	11.5547	14.3519	9.0675	11.7773	14.9239	9.0675	11.3894	14.0064	9.0675	11.2819	13.7119	9.0675	10.8436	12.7029
	60°	8.7568	11.2636	14.0947	8.7568	11.4796	14.6552	8.7568	11.0758	13.6946	8.7568	10.9721	13.4100	8.7568	10.5410	12.4135
	90°	5.3535	7.7117	13.0147	5.3535	7.84022	13.5520	5.3535	7.65212	12.5115	5.3535	7.63944	12.1914	5.3535	7.33930	11.2717
1.0	30°	6.3706	7.9684	9.6526	6.3706	8.1467	10.0951	6.3706	7.8721	9.4971	6.3706	7.7648	9.2313	6.3706	7.4746	8.5772
	45°	6.1143	7.6739	9.3836	6.1143	7.8331	9.7832	6.1143	7.5859	9.2170	6.1143	7.5034	9.0049	6.1143	7.2191	8.3564
	60°	5.8025	7.3617	9.0971	5.8025	7.51068	9.4767	5.8025	7.2581	8.8861	5.8025	7.1832	8.6878	5.8025	6.9068	8.0535
	90°	3.3115	4.2592	8.1185	3.3115	4.3619	8.4473	3.3115	4.1814	7.8169	3.3115	4.1082	7.6018	3.3115	3.9539	7.0286

30° inclination and at a minimum for 90° inclination. The local Nusselt number is seen to decrease as the inclination angle increases in the case of constant heat flux being applied through the left sidewall ($\varepsilon = 1.0$).

The changes in local Nusselt number for water-based copper nanofluids at $Ra = 10^4$ and 10^6 for several values of solid volume fractions, at the heated wall where constant heat flux is being applied both partially and through the entire wall, are shown in Figs. 10 and 11. As the Rayleigh number increases, the circulation strength increases as a result of higher buoyancy forces. This results in an increase of the local Nusselt number. As a result of the stronger circulation produced by elevated thermal energy transport, the local Nusselt number takes on higher values with increasing solid volume fractions. The local Nusselt number decreases while the length of the heater increases.

The changes in local Nusselt number for different types of nanoparticles are shown in Fig. 12 (where constant heat flux is applied through the wall). The value of the local Nusselt number decreases according to the following ordering of nanoparticles: Ag, Cu, CuO, Al_2O_3 and TiO_2, since the nanofluids based on solid particles with higher thermal conductivity, increase the rate of heat transfer more significantly.

The variations of the average Nusselt number with the Rayleigh number are shown in Tables 5 and 6 for various values of the governing parameters. The average heat transfer rate takes on values that decrease according to the ordering Ag, Cu, CuO, Al_2O_3, and TiO_2. The average Nusselt number does not show a significant increase with an increase in the solid volume fraction for low *Ra* numbers, as a result of the weak convection in this regime. On the other hand, for high *Ra* numbers, there is a remarkable increase in heat transfer with increasing solid volume fraction. As can be seen from Table 6, while the heater length increases, the average heat transfer rate starts to decrease for smaller inclination angles. For example, the rate starts to decrease at 90° for $\varepsilon = 0.25$, 60° for $\varepsilon = 0.50$, 45° for $\varepsilon = 1.0$, respectively. The maximum rate of heat transfer takes place at $\varphi = 30°$, and the minimum rate of heat transfer takes place for $\varphi = 90°$.

5. Conclusion

This paper examines the heat transfer enhancement of water-based nanofluids in a two-dimensional inclined enclosure with a constant flux heater numerically for a range of inclination angles, nanoparticles, solid volume fractions, heat source lengths and Rayleigh numbers. The results show that the presence of nanoparticles causes a substantial increase in the heat transfer rate. The results also illustrate that, as the solid volume fraction increases, the effect is more pronounced. As expected, nanoparticles with a higher thermal conductivity (such as Ag and Cu) produce a greater enhancement in the rate of heat transfer. The variation of the average Nusselt number is nearly linear with the solid volume fraction. The length of the heater also affects heat transfer, the latter decreasing with an increase in the length of the heater. While the heater length is increased, the average heat transfer rate actually starts to decrease for smaller inclination angles. For example, the rate starts to decrease at 90° for $\varepsilon = 0.25$, 60° for $\varepsilon = 0.50$, 45° for $\varepsilon = 1.0$, respectively. The maximum heat transfer takes place at $\varphi = 30°$, and the minimum heat transfer takes place at $\varphi = 90°$.

References

[1] J.A. Eastman, S.U.S. Choi, S. Li, W. Yu, L.J. Thompson, Anomalously increased effective thermal conductivities of ethylene glycol-based nanofluids containing copper nanoparticles, Appl. Phys. Lett. 78 (2001) 718–720.

[2] S.U.S. Choi, Enhancing thermal conductivity of fluids with nanoparticles, in: D.A. Siginer, H.P. Wang (Eds.), Developments and Applications of Non-Newtonian Flows, FED-vol. 231/MD-vol. 66, ASME, New York, 1995, pp. 99–105.

[3] P. Keblinski, S.R. Phillpot, S.U.S. Choi, J.A. Eastman, Mechanisms of heat flow in suspensions of nano-sized particles (nanofluids), Int. J. Heat Mass Transfer 45 (2002) 855–863.

[4] R.L. Hamilton, O.K. Crosser, Thermal conductivity of heterogeneous two-component systems, I & EC Fundamentals 1 (1962) 182–191.

[5] F.J. Wasp, Solid–Liquid Flow Slurry Pipeline Transportation, Trans. Tech. Publ., Berlin, 1977.

[6] J.C. Maxwell-Garnett, Colours in metal glasses and in metallic films, Philos. Trans. Roy. Soc. A 203 (1904) 385–420.

[7] D.A.G. Bruggeman, Berechnung verschiedener physikalischer konstanten von heterogenen substanzen, I. Dielektrizitatskonstanten und Leitfahigkeiten der Mischkorper aus Isotropen Substanzen, Ann. Physik. Leipzig 24 (1935) 636–679.

[8] B.X. Wang, L.P. Zhou, X.F. Peng, A fractal model for predicting the effective thermal conductivity of liquid with suspension of nanoparticles, Int. J. Heat Mass Transfer 46 (2003) 2665–2672.

[9] W. Yu, S.U.S. Choi, The role of interfacial layers in the enhanced thermal conductivity of nanofluids: a renovated Maxwell model, J. Nanoparticle Res. 5 (2003) 167–171.

[10] K. Khanafer, K. Vafai, M. Lightstone, Buoyancy driven heat transfer enhancement in a two-dimensional enclosure utilizing nanofluids, Int. J. Heat Mass Transfer 46 (2003) 3639–3653.

[11] R.Y. Jou, S.C. Tzeng, Numerical research of nature convective heat transfer enhancement filled with nanofluids in rectangular enclosures, Int. Commun. Heat Mass Transfer 33 (2006) 727–736.

[12] A.K. Santra, S. Sen, N. Chakraborty, Study of heat transfer augmentation in a differentially heated square cavity using copper–water nanofluid, Int. J. Thermal Sci. 47 (2008) 1113–1122.

[13] K.S. Hwang, J.H. Lee, S.P. Jang, Buoyancy-driven heat transfer of water-based Al_2O_3 nanofluids in a rectangular cavity, Int. J. Heat Mass Transfer 50 (2007) 4003–4010.

[14] S.P. Jang, S.U.S. Choi, The role of Brownian motion in the enhanced thermal conductivity of nanofluids, Appl. Phys. Lett. 84 (2004) 4316–4318.

[15] H.F. Oztop, E. Abu-Nada, Numerical study of natural convection in partially heated rectangular enclosures filled with nanofluids, Int. J. Heat Fluid Flow 29 (2008) 1326–1336.

[16] F.P. Incropera, Convection heat transfer in electronic equipment cooling, J. Heat Transfer 110 (1988) 1097–1111.
[17] I.E. Sarris, I. Lekakis, N.S. Vlachos, Natural convection in rectangular tanks heated locally from bellow, Int. J. Heat Mass Transfer 47 (2004) 3549–3563.
[18] B. Calgagni, F. Marsili, M. Paroncini, Natural convective heat transfer in square enclosures heated from below, Appl. Therm. Eng. 25 (2005) 2522–2531.
[19] O. Aydın, W.J. Yang, Natural convection in enclosures with localized heating from below and symmetrical cooling from sides, Int. J. Numer. Meth. Heat Fluid Flow 10 (2000) 518–529.
[20] M.A.R. Sharif, T.R. Mohammad, Natural convection in cavities with constant flux heating at the bottom wall and isothermal cooling from the sidewalls, Int. J. Therm. Sci. 44 (2005) 865–878.
[21] N.B. Cheikh, B.B. Beya, T. Lili, Influence of thermal boundary conditions on natural convection in a square enclosure partially heated from below, Int. Commun. Heat Mass Transfer 34 (2007) 369–379.
[22] H.C. Brinkman, The viscosity of concentrated suspensions and solutions, J. Chem. Phys. 20 (1952) 571–581.
[23] Y. Xuan, W. Roetzel, Conceptions for heat transfer correlation of nanofluids, Int. J. Heat Mass Transfer 43 (2000) 3701–3707.
[24] C. Shu, K.H.A. Wee, Numerical simulation of natural convection in a square cavity by SIMPLE-generalized differential quadrature method, Comput. Fluids 31 (2002) 209–226.
[25] Y.D. Zhu, C. Shu, J. Qiu, J. Tani, Numerical simulation of natural convection between two elliptical cylinders using DQ method, Int. J. Heat Mass Transf. 47 (2004) 797–808.
[26] M.C. Ece, E. Büyük, The effect of an external magnetic field on natural convection in an inclined rectangular enclosure, Proc. Inst. Mech. Eng., Part C, J. Mech. Eng. Sci. 221 (2007) 1609–1622.
[27] C. Shu, Differential Quadrature and its Application in Engineering, Springer and Verlag, 2000.
[28] R.E. Belman, B.G. Kashef, J. Casti, Differential quadrature: a technique for the rapid solution of nonlinear partial differential equations, J. Comput. Phys. 10 (1972) 40–52.
[29] C. Shu, Generalized differential–integral quadrature and application to the simulation of incompressible viscous flows including parallel computation, PhD thesis, University of Glasgow, 1992.
[30] C. Shu, B.E. Richards, Application of generalized differential quadrature to solve two-dimensional incompressible Navier Stokes equations, Int. J. Numer. Meth. Fluids 15 (1992) 791–798.
[31] K. Kahveci, Numerical simulation of natural convection in a partitioned enclosure using PDQ method, Int. J. Numer. Meth. Heat Fluid Flow 17 (4) (2007) 439–456.
[32] K. Kahveci, Natural convection in a partitioned vertical enclosure heated with a uniform heat flux, ASME J. Heat Transfer 129 (2007) 717–726.
[33] K. Kahveci, A differential quadrature solution of natural convection in an enclosure with a finite thickness partition, Numer. Heat Trans. Part A: Appl. 51 (10) (2007) 979–1002.
[34] G. de Vahl Davis, Natural convection of air in a square cavity: a benchmark numerical solution, Int. J. Numer. Meth. Fluids 3 (1983) 249–264.